IEEE Journal of Microwaves

Received 7 March 2022; revised 2 June 2022 and 21 July 2022; accepted 21 July 2022. Date of publication 11 August 2022; date of current version 7 October 2022.

Digital Object Identifier 10.1109/JMW.2022.3194062

Transmitter and Receiver in 0.13 μm SiGe for Gas Spectroscopy at 222–270/444–540 GHz

KLAUS SCHMALZ [1], ALEXANDRA GLÜCK [2,3], NICK ROTHBART [2,3], ALPER GÜNER [1], MOHAMED HUSSEIN EISSA [1], AND HEINZ-WILHELM HÜBERS [2,3]

(Regular Paper)

[1]IHP—Leibniz-Institut für Innovative Mikroelektronik, 15236 Frankfurt, Germany
[2]Institute of Optical Sensor Systems, German Aerospace Center (DLR), 12489 Berlin, Germany
[3]Department of Physics, Humboldt-Universität zu Berlin, 12489 Berlin, Germany

CORRESPONDING AUTHOR: Mohamed Hussein Eissa (e-mail: eissa@ihp-microelectronics.com).

This work was supported by Deutsche Forschungsgemeinschaft (DFG) through the DFG Project ESSENCE under Grant SPP 1857.

ABSTRACT This paper presents a transmitter (TX) and a receiver (RX) with a cross-polarized bowtie-antenna on a silicon lens for gas spectroscopy at 222–270 GHz and the doubled frequency at 444–540 GHz. TX and RX are fabricated in 0.13 μm SiGe BiCMOS technology. Both use two integrated local oscillators for frequency subbands 222–256 GHz and 250–270 GHz, which allow operating in one branch of the TX and RX at 222–270 GHz and in a second branch of the TX and RX at 444–540 GHz by frequency doubling. The directivity of the cross-polarized bowtie-antenna of the TX and RX is optimized for these two frequency bands with an estimated value of 24.4 dBi at 260 GHz, and 29.5 dBi at 520 GHz. Absorption spectroscopy of gaseous methanol is used as a measure for the performance of the TX and RX in the lower and upper frequency bands.

INDEX TERMS Bowtie antenna, gas spectroscopy, mm-wave, receiver, SiGe, terahertz, transmitter.

I. INTRODUCTION

High-resolution spectroscopy at the range of millimeter-wave (mmW)/terahertz (THz) frequencies is a very effective technique for gas sensing, because many molecules have rotational transitions in this range [1]–[3]. Advanced SiGe BiCMOS or CMOS technologies for mmW/THz applications, which are now available, allow building compact systems for gas spectroscopy at low cost.

A 220–320 GHz spectrometer has been described, which consists of a pair of 65 nm CMOS chips and utilizes two frequency-comb signals with ten equally spaced frequency tones to scan the spectrum [4], [5]. Furthermore, a transmitter (TX) and receiver (RX) in 65 nm CMOS have been reported [6]–[8], with gas spectroscopy results at 225-255 GHz [8].

A 28 nm CMOS TX for pulsed operation at 180 GHz has been designed for in-situ molecular sensing in planetary science [9]. A complete 183 GHz CMOS/InP hybrid heterodyne-spectrometer with an InP low noise amplifier, a 28 nm CMOS RX and a 65 nm CMOS spectrometer has been recently realized for spaceborne atmospheric remote sensing applications [10].

Many gas molecules have stronger absorption lines at higher frequencies than around 240 GHz. Thus, extension of the bandwidth to the range around 480 GHz can increase sensitivity and selectivity for gas sensing. For instance, the strongest absorption of formaldehyde (CH_2O) around 480 GHz is by a factor of 10 stronger compared to the strongest transition in the band centered at 240 GHz band. H_2O (water vapor) can be detected at 448 GHz. The frequency range around 480 GHz also allows to detect hydrogen sulfide (H_2S) (e.g., at 493.36 GHz), nitrogen dioxide (NO_2) (e.g., at 493.28 GHz), and sulfur dioxide (SO_2) (e.g., at 491.93 GHz) more efficiently than at lower frequencies.

A digital-to-impulse radiating array in 65 nm CMOS was used as an electronic source with an on-chip antenna to perform broadband THz gas spectroscopy for NH_3 (ammonia) at 572 GHz, and H_2O at 753 GHz, respectively, with gas pressure at 500-950 Torr [11]. Further, the same group reported a chip in 0.13 μm SiGe BiCMOS which radiates 1.7-ps pulses

via an on-chip antenna resulting in a broadband 0.1–1.1 THz frequency comb [12].

We reported previously a narrowband 500 GHz TX/RX system in SiGe BiCMOS for gas spectroscopy of a methanol (CH_3OH)/acetonitrile (CH_3CN) mixture at 495–497 GHz [13], [14], and demonstrated TXs and RXs, fabricated in IHP's 0.13 μm SiGe BiCMOS, with integrated antennas for gas spectroscopy at 238–252 GHz [15]–[18]. The design of the TX- and RX-circuits is described in detail in [19]–[24]. A 2-band TX-chip and a 2-band RX-chip were reported, which were implemented by combining two TX- and two RX-circuits with their own on-chip antennas on corresponding single chips to realize an effective bandwidth of 222–270 GHz for a gas spectroscopy system [25]. LBE (Localized Backside Etching) technology, which is available at IHP, was used to realize on-chip antennas with high efficiency.

Our previous paper, [26] describes the implementation of a single bowtie-antenna with silicon lens for a 2-band TX and RX, increasing their performance parameters considerably compared to the former 2-band TX and RX with two separate LBE on-chip antennas, [25].

To extend the frequency range of our gas spectroscopy system, we developed TX- and RX-subcircuits for the frequency band around 480 GHz. A 4-way combined frequency multiplier chain in 0.13μm SiGe BiCMOS was presented, which converts a single ended 110–135 GHz input signal to a differential 440–540 GHz output signal [27]. It uses four identical multiplier chains with two frequency doubling stages. Further, a subharmonic mixer (SHM) in 0.13μm SiGe BiCMOS was reported with measured results for the range 450–500 GHz, which uses a single-balanced topology [28].

The present work is aimed to extend the frequency coverage of our previous 240 GHz gas spectroscopy system in SiGe BiCMOS, [26] by developing a two-band sensor system, which covers simultaneously the frequency band of 222–270 GHz and the band at the doubled frequencies of 444–540 GHz, and thus to achieve a considerably wider bandwidth as compared to our former 495–497 GHz system.

This goal is realized by implementing an integrated cross-polarized antenna on silicon-lens with high directivity for these two frequency ranges of the TX and RX, and by using a 240 GHz branch of TX/RX subcircuits in parallel with a corresponding 480 GHz branch for the TX and RX.

The paper is organized as follows: The TX- and RX-chips for the frequency band around 240 GHz, and the doubled frequencies around 480 GHz with their dual-polarized bowtie-antenna with silicon lens are reported in Section II. System aspects and results of gas spectroscopy are presented in Section III. Section IV provides a discussion of the system performance. The conclusion of the paper gives an outlook concerning further improvement of our TX/RX system.

II. TRANSMITTER AND RECEIVER

The TX and RX were implemented in IHP's SG13G2 technology, which is a 0.13 μm SiGe BiCMOS technology with a very high bipolar performance of f_T/f_{max} = 300/500 GHz. The backend option offers five thin metal layers (Metal1–Metal5), two thick metal layers (TopMetal1 and TopMetal2, 2 and 3 μm thick), as well as metal-insulator-metal layer between Metal5 and TopMetal1 [29].

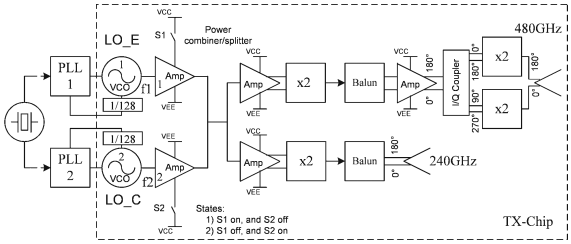

FIGURE 1. Block diagram of the 2-band transmitter with the two frequency bands 222–270 GHz and 444–540 GHz.

The TX and RX use two integrated local oscillators (LOs), which are combined by a Wilkinson power combiner and switched for two-subband (222–256 GHz and 250–270 GHz) operation, see Fig. 1, as described in [26]. The combined LO signal is split by a Wilkinson power splitter into two branches: (i) the lower one for operation on 222–270 GHz, and (ii) the upper one for operation at the doubled frequencies of 444–540 GHz.

A silicon-lens integrated cross-polarized antenna combines two antennas designed for the two frequency bands 222–270 GHz and 444–540 GHz, respectively, with minimal coupling between both. This ensures the same alignment of the corresponding two radiated beams for both frequency bands with a high antenna gain to perform gas spectroscopy for these frequency bands with the same setup.

A. TRANSMITTER FOR TWO FREQUENCY BANDS

Fig. 1 depicts the block diagram of the TX, where in the lower branch the single-ended output of the 240 GHz frequency doubler is connected to a differential 240 GHz bowtie-antenna by a balun, and in the upper branch the two outputs with opposite phases of the two frequency doublers are connected to a differential 480 GHz bowtie antenna.

The LO consists of a push-push voltage controlled oscillator (VCO) with a frequency divider and a differential two stage power amplifier, [30]. The divider ratio of 1/128 is due to the 1/64 frequency divider applied for the fundamental frequency of the used push-push oscillator. The LO-frequency is tuned by an external PLL. Two LOs (LO_C and LO_E, see Fig. 1) with the tuning ranges 111–128 GHz and 125–135 GHz, respectively, are used.

The layout of the Wilkinson power splitter is identical with the one of the Wilkinson power combiner. This power combiner exhibits a simulated insertion loss of 1.5 dB at 120 GHz and more than 20 dB of isolation [26].

The split power signal is connected to both branches through a power amplifier (measured gain is 19 dB at 120 GHz) to a 240 GHz frequency doubler with single-ended output, [30]. For the upper branch, the frequency of the single ended signal is doubled, [27]. First, the signal of the 240 GHz

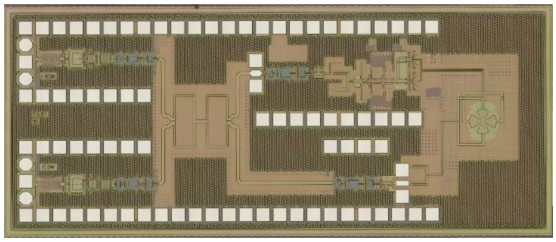

FIGURE 2. Photograph of the 2-band transmitter-chip with cross-polarized antenna. The details are described in the block diagram of the TX.

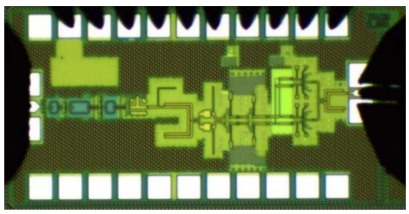

FIGURE 3. Photograph of the single-band transmitter chip (upper frequency band) without antenna.

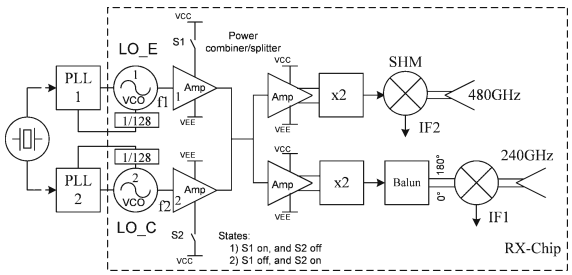

FIGURE 4. Block diagram of the 2-band receiver with the two frequency bands 222–270 GHz and 444–540 GHz.

frequency doubler is transformed into a differential one by a Marchand balun and amplified with a 2-stage differential cascode amplifier. Then, its quadrature components are obtained by a quadrature (I/Q) coupler, which are applied to two frequency doublers to obtain a balanced signal at the doubled frequency.

Fig. 2 shows the photograph of the 2-band TX-chip with its cross-polarized antenna consisting of two bowtie-antennas corresponding to the 240 GHz frequency band (connected to the lower 240 GHz TX branch) and the 480 GHz band (connected to the upper 480 GHz TX branch), respectively. The area of the TX-chip is 3.2×1.33 mm^2. Fig. 3 presents the photograph of the test-chip, which allowed to measure on-wafer the output power of the upper TX-branch by using an external LO at the input of the 120 GHz power amplifier. Here, a Marchand balun (see [27]) combines the two single-ended outputs of the frequency doublers having opposite phases. The area of this test-chip is 1.2×0.65 mm^2.

B. RECEIVER FOR TWO FREQUENCY BANDS

Fig. 4 depicts the block diagram of the 2-band RX. The two LOs (LO_C and LO_E), their combination by a Wilkinson

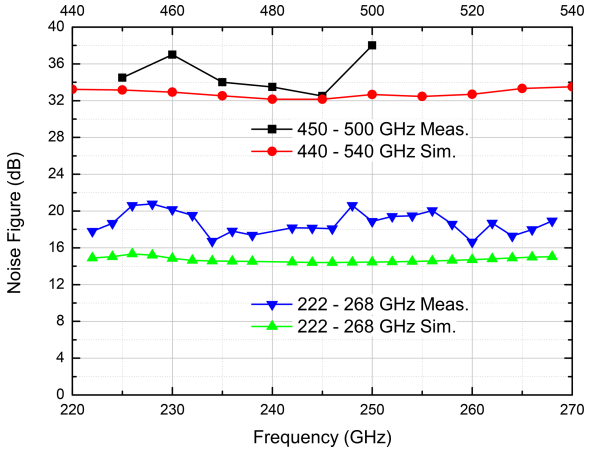

FIGURE 5. Measured and simulated NF values for the two frequency bands 222–270 GHz and 444–540 GHz.

power combiner, and the split power signal is connected for both branches through a power amplifier as described above for the TX. In the RX-chip the same frequency doubler was used as in the TX-chip. In the lower branch the frequency-doubled LO signal is then applied through a Marchand balun to the 240 GHz mixer, [31], [32], which is connected to the differential bowtie-antenna for the lower frequency band. In the upper branch the frequency-doubled LO signal is connected to the 480 GHz single-balanced subharmonic mixer [28], being directly connected to the differential bowtie-antenna for the upper frequency band.

The dc offset cancellation loop architecture of the 240 GHz mixer and biasing purposes are described in [31]. This reported 220–275 GHz RX core (without internal LO) achieves a 3 dB bandwidth of 55 GHz, with a conversion gain of 13 dB. The noise figure (NF) was measured using the gain method. The average single-sideband (SSB) NF is 18 dB [31].

The 480 GHz subharmonic mixer was measured within the RF range of 450–500 GHz using a Marchand balun for the differential RF input [28]. The NF measurement was performed with the gain method by measuring the IF output noise floor [28]. The measured conversion loss is 8.5 dB and the measured NF is 33 dB at 480 GHz for -1 dBm of LO-power. The measured conversion loss is in the range of 7.5-12.5 dB at 450–500 GHz. Fig. 5 shows the measured and simulated NF values for both frequency bands 222–270 GHz and 444–540 GHz.

Fig. 6 shows the photograph of the 2-band RX-chip with its cross-polarized antenna consisting of two bowtie-antennas corresponding to the 240 GHz frequency band (connected to the lower 240 GHz RX branch) and the 480 GHz band (connected to the upper 480 GHz RX branch), respectively. The area of the RX-chip is of 3.2×1.64 mm^2.

C. CROSS-POLARIZED BOWTIE ANTENNA

The layout of the designed cross-polarized bowtie-antenna is shown in Fig. 7.

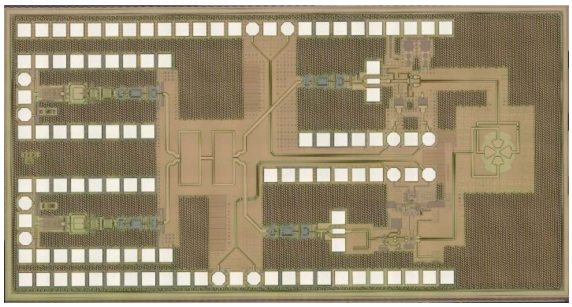

FIGURE 6. Photograph of the 2-band receiver-chip with cross-polarized antenna. The details are described in the block diagram of the RX.

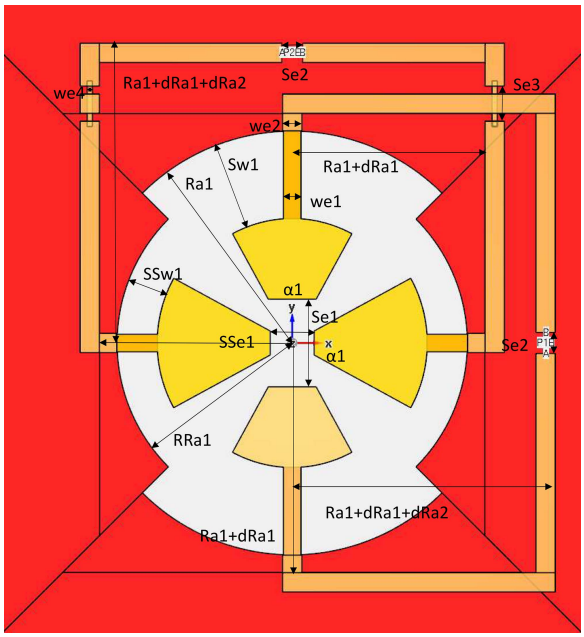

FIGURE 7. Layout of the designed cross-polarized antenna.

The antenna is implemented using the top Al metallization layer (TopMetal2) with a thickness of 3 μm and Metal3 for the ground layer. The crossing between the two feed lines is realized in TopMetal1 (thickness of 2 μm). The thickness of the 50 ohm·cm silicon substrate with the BEOL (backend-of-the-line layer) stack on top is 200 μm. A hyper-hemispherical silicon lens is attached to the backside of the silicon substrate.

The antenna design is based on a broadband 240 GHz lens-integrated polarization-diversity on-chip circular slot antenna, [33]–[35]. We modified this design for a cross-polarized operation at 220-270 GHz and 440–540 GHz. We obtained the following optimum layout parameters (see Fig. 7) for the parameterized antenna model using ANSYS HFSS, [36] simulations (length in μm): α1=57.3°, Ra1=121, Sw1=50, Se1=50, dRa1=10, we1=10, dRa2=40, we2=11, Se2=12, Se3=20, we4=3, RRa1=100, SSw1=23, SSe1=25. Ground insets in Metal3 with a width of w3=10μm, and a length le1=Sw1 and lle1=SSw1, respectively, are located underneath the feed lines of both bowtie antennas.

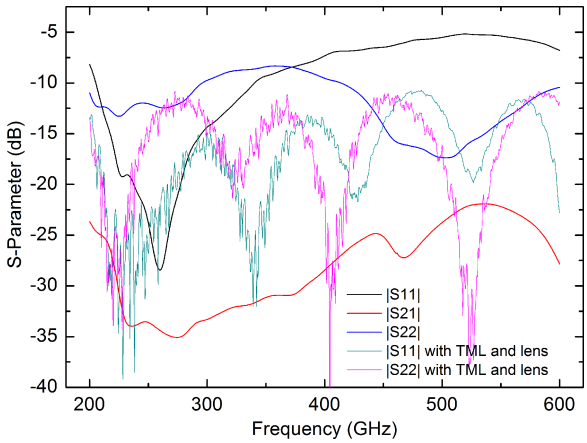

FIGURE 8. Simulated S-parameters of the cross-polarized bowtie antenna.

The antenna with the silicon lens was also simulated using a Finite Difference Time Domain (FDTD) based 3D EM field solver software, EMPIRE XPU [37] to optimize the parameters of the silicon lens and to comply with the metal density rules of IHP's SG13G2 technology. The parameters of the silicon lens are optimized to realize a high directivity for both frequency bands. A hyper-hemispherical lens with a diameter of 6 mm and an extension of 0.8 mm is used without anti-reflection coating.

Fig. 8 shows the simulated S11, S22, and S21 of the designed antenna, depicted in Fig. 7, assuming an absorbing boundary at the backside of the silicon substrate (for condition of infinite thickness). Sufficient matching with |S11| and |S22| < -15 dB is realized for the specified frequency bands of 220-270 GHz for port1 (connected to the smaller bowtie antenna), and 440–540 GHz for port2 (connected to the larger bowtie antenna) with a reference impedance of 100 ohm, and the coupling between port1 and port2 is with |S21| < −22 dB low. The S-parameters are also simulated for the case that differential transmission lines (TML) in TopMetal2 (width of metal line w = 3.5 μm, spacing between the two metal lines s = 5.0 μm) are connected to the antenna, see Fig. 2 for the TX-chip, and with an attached silicon lens (diameter of 6 mm, extension length of 0.8 mm), showing also sufficient matching for port1 and port2.

The antenna with its two bowtie structures is optimized for backside radiation through the silicon substrate and silicon lens. Fig. 9 shows the simulated maximum directivity at this direction for the port1 and port2 of the cross-polarized bowtie antenna, corresponding to the frequency bands 220-270 GHz and 440–540 GHz, respectively. For the lower frequency band, the simulated directivity is in the range 21.0-22.5 dBi, and for the upper frequency band at 24.4-25.6 dBi.

Table 1 presents the antenna efficiency for the port1 at 240 GHz and for the port2 at 480 GHz for the antenna without the connected differential transmission line (TML), and for the antenna with connected TML for two parameters sets of the width w of metal line, and the spacing s between the two metal lines. We used the TML with w=3.5 μm and s=5μm. Here,

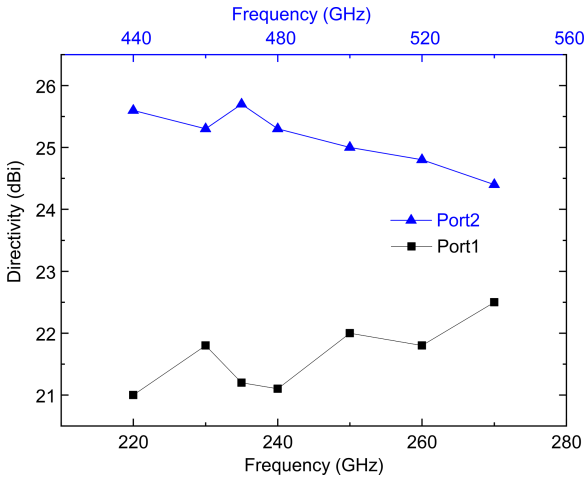

FIGURE 9. Simulated directivity of the cross-polarized bowtie antenna for port1 (220-270 GHz) and port2 (440–540 GHz).

TABLE 1. Simulated Antenna Efficiency of the Antenna

Transmission line (TML) at antenna	Port1 240 GHz	Port2 480 GHz
without TML	-1.0 dB	-1.1 dB
with TML, in this work: w=3.5µm, s=5µm	-4.3 dB	-5.3 dB
with TML w=7µm, s=10µm	-1.8 dB	-2.3 dB

w- width, s- spacing of differential TML, port1 –corresponding to smaller bowtie, and port2 corresponding to larger bowtie antenna.

the simulated antenna efficiency is −4.3 dB at 240 GHz and −5.3 dB at 480 GHz, respectively. However, a higher antenna efficiency of about −2 dB could be realized by the broader TML.

D. TRANSMITTER- AND RECEIVER MODULES

The TX/RX chips were bonded on plug-in boards, which were plugged on baseband boards using plugs on the adapter board and corresponding sockets on the baseband board [26]. The baseband board contains multiple switchable linear voltage regulators to supply all of the chips' bias voltages from a single 5 V DC supply. The two PLL devices (Analog Devices ADF4169) are integrated in the baseband board. A PLL loop bandwidth of 100 kHz is implemented. The frequency bands of the TX can be switched electronically by switching the LOs and power amplifiers of the TX- and RX-chips on and off, respectively. This allows realizing a bandwidth of the lower frequency band of almost 50 GHz for the spectroscopy system, and to select the frequency band around 240 GHz or around the doubled frequency of 480 GHz with a bandwidth of almost 100 GHz. An internal reference clock of 100 MHz is placed on the baseband board to allow synchronization of the four fractional-N PLLs, and it is used as an external reference clock for the experimental setup.

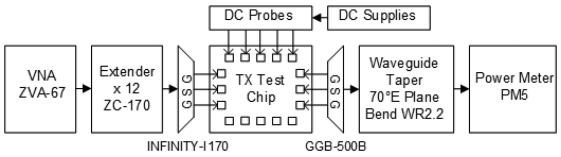

FIGURE 10. Characterization setup for on-wafer measurements of the TX test-chip without antenna.

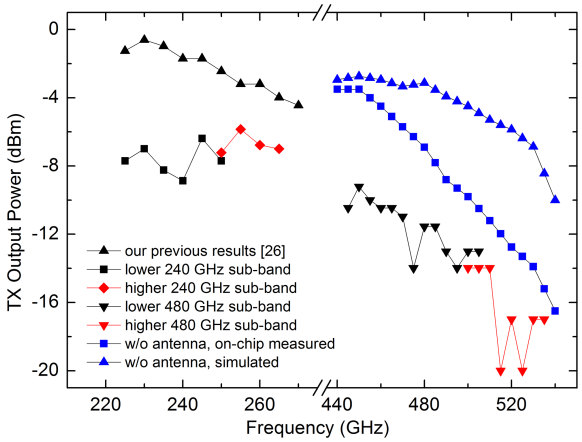

FIGURE 11. Radiated and on-chip TX output-power versus frequency.

E. RESULTS ON THE TRANSMITTER

The on-wafer measurement setup for the TX test-chip (see Fig. 3) is shown in Fig. 10, and is described including its calibration in [27].

The input signal to the TX-chip of 110-135 GHz is provided by a Rohde & Schwarz (R&S) ZC-170 frequency extender, which is connected to a 9.16-11.25 GHz input signal of the R&S vector network analyzer (VNA). The output power of the extender is measured through the VNA using the internal power sensor of the extender. The output signal is connected to a R&S 70° E plane bend and a WR2.2-to-WR10 PM5 taper connection to measure the output power at 440–540 GHz with a PM5 power meter. The total loss of this connection is calculated as 2 dB, 1.4 dB from the bend and 0.6 dB from the taper. The calibration data of the GGB-500B probe is also considered for the output power.

As a reference, the radiated power was measured in free-space as well for the two frequency bands. This measurement was performed with a Thomas Keating power meter. The TX was placed in a distance of 5 cm to the power meter to collect the power from the whole antenna profile. A chopper wheel between TX and power meter provided the modulation required for the power meter usage. The power was measured over the whole frequency range of the TX in steps of 5 GHz.

Fig. 11 illustrates the output power of the single-band TX test-chip, measured on-wafer compared to the simulated output power of the single-band TX test-chip, and TX radiated output power versus the TX frequency.

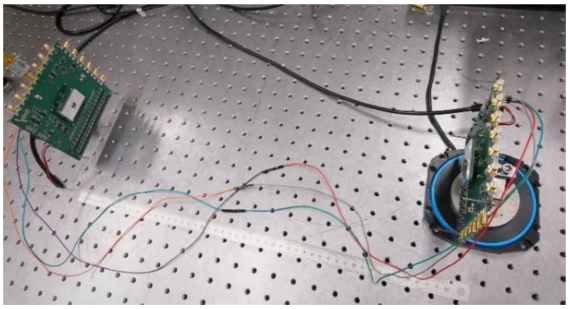

FIGURE 12. Photo of the setup with TX- and RX-modules for radiation pattern measurements.

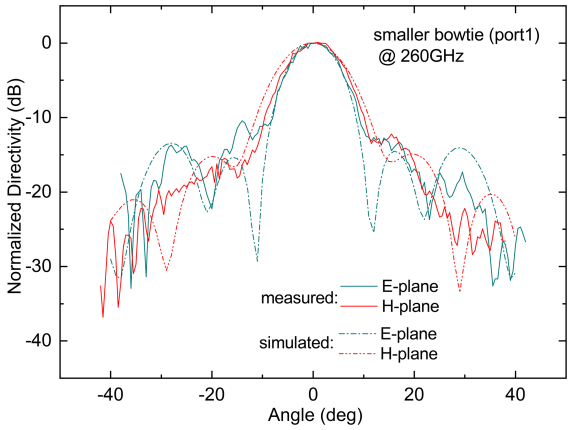

FIGURE 13. Measured and simulated and measured radiation patterns at 260 GHz (distance of 50 cm between TX and RX, IF= 150 MHz).

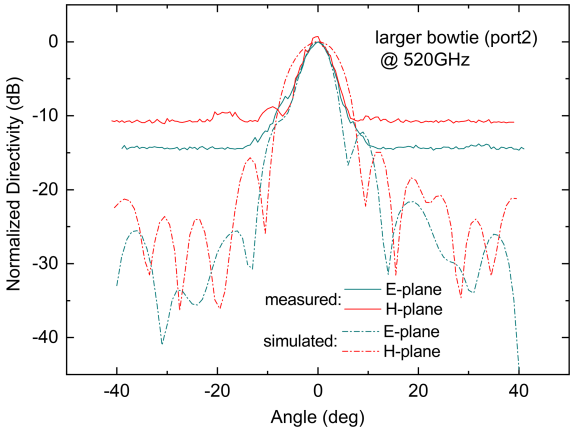

FIGURE 14. Measured and simulated radiation patterns at 520 GHz (distance of 50 cm between TX and RX, IF= 150 MHz).

The TX test-chip delivers an on-chip output power of −3.5 dBm at 445 GHz, and of −7.5 dBm at 480 GHz. The simulated and measured values agree at 445 GHz, but they disagree at higher frequencies. This disagreement indicates probably a limitation of the used transistor models for this frequency range.

Excluding the loss of the Marchand balun on the output of the TX test-chip (the Marchand balun was not used for the 2-band TX chip), the corrected output power would amount −2 dBm and −5 dBm at these frequencies, respectively. The radiated TX output power agrees with the corrected on-chip output power, if taking into account the simulated efficiency of the bowtie antenna of -5.3 dB (see Table 1), and a simulated 2 dB decrease of output power at 65 °C due to self-heating of the TX-chip on the TX-module. The scatter of power values at frequencies around 520 GHz indicates an essential uncertainty problem for these low values, because it is close to the limit of detection of the TK power meter.

Fig. 11 presents also the corresponding results of our previous TX for the lower frequency band [26]. These results agree for the higher subband with the measured data, if considering the different antenna efficiencies of −4.3 dB for the present TX, and −1.9 dB (65%) for the previous TX, [26]. For the lower subband (222–256 GHz) the TX power is lower than the expected 2.4 dB difference to our previous results, [26].

Fig. 12 depicts the setup with the TX- and RX-modules used for the radiation pattern measurements.

Figs. 13 und 14 show the normalized simulated results and measured radiation pattern at 260 GHz (Fig. 12) and 520 GHz (Fig. 14) for the E-plane and for the H-plane, respectively. For the smaller bowtie (radiating at 260 GHz) the E-plane coincidences with YZ-plane and the H-plane with XZ-plane, and for the larger bowtie (radiating at 520 GHz) the E-plane coincidences with the XZ-plane and the H-plane with the YZ-plane, see Fig. 7. To determine the TX antenna profiles experimentally, we mounted the TX-module on a rotation stage and placed the RX-module in a distance of 50 cm where it is reasonable to assume far-field conditions. The TX was rotated by 180° in 0.5° steps. This was carried out for TX frequencies of 235 GHz, 470 GHz, 260 GHz and 520 GHz. The RX was set to the respective frequency +150 MHz and the maximum of the IF-signal was measured with a spectrum analyzer. This measurement was performed for both, the E- and H-plane.

The measured radiation pattern at 260 GHz with a dynamic range of about 30 dB correlates well with the simulated one concerning the main lobe and the side lobes, see Fig. 13. Due to the lower dynamic range of 10-15 dB for the power measurement at 520 GHz, the side lobes were not resolved in the radiation pattern and only the main lobe was detected, see Fig. 14. Note, that our EMPIRE simulations considered the antenna structure including the connected transmission lines by importing the layout designed by Cadence Virtuoso software [38], but without filler structures. By using a Gaussian fit for the measured main lobe [26], we estimated the Full Width at Half Maximum (FWHM) angles for the E- and H-planes.

From FWHM angles, the directivity of the cross-polarized bowtie antenna was estimated for selected frequencies by using the approximation $D = 29000/(\theta_x\ \theta_y)$ for narrow beams [39]. The estimated values of the directivity are somewhat larger than the simulated ones, see Table 2.

TABLE 2. FWHM Angles Derived by Fits in Horizontal (E-Plane) and Vertical (H-Plane) Direction, Corresponding Simulated FWHM Angles, Estimated Directivity, and Simulated directivity. The Measurements Were Performed With a Distance of 50 cm Between the TX and the RX, and With an IF-frequency of the RX at 150 MHz

Freq. (GHz)	E/H Pl.	Meas. FWHM	Estimat. Dir. (dBi)	Simul. FWHM	Simulated Dir. (dBi)
235	E	11.1°	23.5	10.2	21.2
	H	11.6°		13.0	
260	E	9.8°	24.4	9.6	22.5
	H	10.8°		11.7	
470	E	6.3°	28.1	6.8	25.8
	H	7.1°		7.7	
520	E	5.6°	29.5	5.2	24.8
	H	5.8°		9.9	

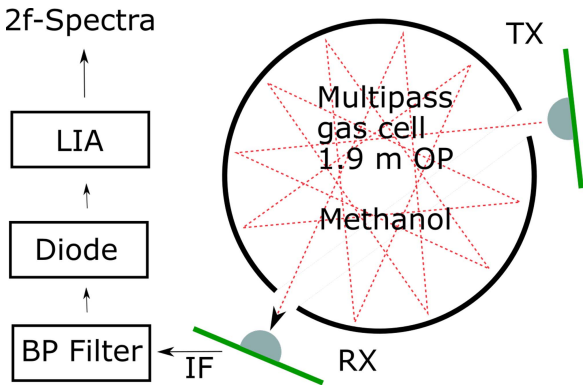

FIGURE 15. Schematic of the setup for measurement of methanol absorption lines. The dashed red line indicates the optical path (OP) inside the gas cell. The IF signal is detected by a diode behind bandpass (BP) filter. With a lock-in amplifier (LIA), the second harmonic (2f) content is isolated.

F. RESULTS ON THE RECEIVER

To estimate the conversion gain of the RX, we measured the intermediate frequency (IF) power at 2150 MHz, obtained from the TX at 235 GHz and 470 GHz, respectively, at different distances to the RX, see Fig. 15. The alignment was slightly adjusted for each frequency. The IF power of the single-ended IF output of the RX was measured after amplifying this signal (with typical gain of 13 dB at 2 GHz) by a low-noise amplifier (CMA-5043+), being mounted on the baseband board. Taking into account the measured IF power of −9.1 dBm for the RX at 235 GHz at a distance of 40 cm, the radiated TX power of −8.2 dBm, the directivity of 23.5 dB, and an antenna efficiency of −4.3 dB (Tables 1 and 2), a received power of −41.7 dBm is obtained according to the Friis transmission equation. Considering the 13-dB gain of the external low-noise amplifier, a conversion gain of 19.6 dB is estimated for the RX without the external amplifier. This is somewhat larger than the conversion gain of 12–13 dB, which was obtained by using on-wafer measurements for the RX core [31]. Because we used only the typical gain of the external low-noise amplifier, the conversion gain obtained by on-wafer measurement is more likely to be true. For the measured IF power of −42.6 dBm for the RX at 470 GHz at a distance of 20 cm, the radiated TX power of −11 dBm (see paragraph E), the directivity of 24.8 dB, and the antenna efficiency of −5.3 dB (Tables 1 and 2), the received power is of −43.9 dBm, and the corrected conversion loss is of 11.7 dB for the RX without the external low-noise amplifier. This value agrees with the conversion loss of 7.5-12.5 dB at 450-500 GHz measured for the subharmonic mixer on-wafer [28].

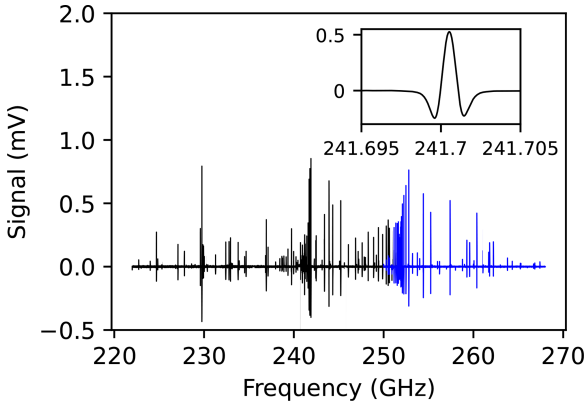

FIGURE 16. Broadband spectrum of methanol measured for the 240 GHz band with the lower subband (black), and the higher subband (blue). The inset displays one line in detail.

III. GAS SPECTROSCOPY SYSTEM

A. GAS SPECTROSCOPY SETUP

The setup of the gas spectroscopy system is based on a circular multi-pass gas cell with a 1.9 m path length as presented in [40], [41], and described in detail in [26]. A schematic of the setup is shown in Fig. 15.

To measure the absorption spectra, the cell was evacuated and then filled with methanol at a pressure of 5 Pa. The frequencies of the TX and RX were tuned over the full frequency range with fixed IF. The step size was 1.22 kHz in the lower frequency range and 2.44 kHz in the upper frequency range. The boards are operated by a baseband board and an SPI interface. The 2.15 GHz IF signal passed a bandpass filter (mini circuits ZX75BP-2150+ wideband bandpass filter covering 2050 to 2250 MHz) and was detected by a diode. The TX frequency was modulated and the second harmonic content of the IF signal was detected by a lock-in amplifier (LIA, Zurich Instruments HF2LI). The resulting spectra follow the shape of the second derivative of the absorption spectrum. The integration time at the lock-in amplifier was 2 ms. In total, it took 2 × 10 minutes to acquire full spectra of both the frequency ranges corresponding to the lower frequency subband, and 2 × 6 min for the two frequency ranges corresponding to the higher frequency subband. Additionally, we measured single lines with an integration time of 16 ms.

B. GAS SPECTROSCOPY RESULTS

Figs. 16 and 17 show the absorption spectra of the two frequency ranges. The second harmonic content of the modulated signal is displayed, which has the shape of the second derivative of the absorption lines. The signal is given in units of

TABLE 3. Parameters of Transmitters and Receivers for Gas Spectroscopy

Parameter	Ref. [4]	Our previous work [26]	This work
Technology	65nm CMOS	0.13µm SiGe BiCMOS	0.13µm SiGe BiCMOS
Freq. Range (GHz)	220-330 10x 10GHz-band	222-270 (2 subbands)	222-270 (2 subbands) 444-540 (2 subbands)
EIRP (dBm) of TX	up to 10	25.2 at 240GHz	17.6 at 260GHz 17.1 at 470GHz
TX/RX-Antenna	Antenna for each band, with silicon lens	Bowtie antenna with silicon lens	Cross-polarized bowtie antenna with silicon lens
Directivity (dBi)	average 10.1	26.7 at 240GHz	23.5 at 235GHz, 24.4 at 260GHz 29.5 at 520GHz
NF of RX (dB) (SSB)	14.6 – 19.5 [a]	18 at 240GHz [a]	18 at 240GHz [a] 33 at 480GHz [a]
IF-outputs	10 for 10 bands	one for 2 subbands	one for 222-270GHz one for 444-540GHz
TX/RX DC Power (W)	1.7/1.7 [b]	0.73/0.93 [c]	1.42/0.89 [c]

[a]measured by the gain method [ ], [b]for TX+RX, [c]only one subband is used.

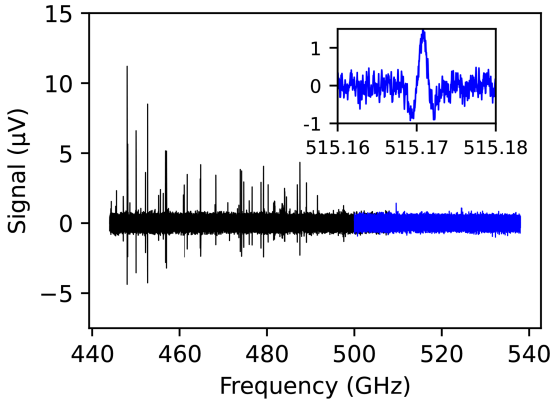

FIGURE 17. Broadband spectrum of methanol measured for the 480 GHz band with the lower subband (black), and the higher subband (blue). The inset displays one line in detail.

mV. In Fig. 16, we removed seven spikes (∼2 MHz width) for clarity, which appeared in the spectrum according to their multiplication factor (256 for the 240 GHz band, and 512 for the 480 GHz band), when the TX divider frequency reached an integer multiple of 20 MHz(originating due to a PLL divider). In Fig. 17, we removed four of these spikes. In both spectra, multiple absorption lines of methanol can be distinguished. At frequencies above 500 GHz, the number of detected lines is strongly reduced, but still multiple lines are visible. With an integration time of 16 ms, the line at 515.17 GHz, which has an line strength of $1.97.10^{-22}$ cm (JPL database), was detected with an SNR of 19 (compare inset in Fig. 17). In the lower frequency range, the absorption line at 241.7 GHz ($4.97.10^{-23}$ cm line strength) has an SNR of 1740 (compare inset in Fig. 16).

IV. DISCUSSION

Table 3 summarizes the main parameters of the TX and RX in SiGe BiCMOS described above as well as those of the previous version [26], and the parameters of TX- and RX-front ends in 65 nm CMOS technology, which were developed for gas spectroscopy [4], [5]. The CMOS based system with its 10 × 10 GHz spectrum acquisition uses for each 10 GHz sub-band its antenna on the silicon lens, and generates 10 IF-outputs of corresponding RX-units. Using a cross-polarized bowtie antenna for the two frequency ranges 222–270 GHz and 444-570 GHz our TX/RX realizes a considerably broader frequency coverage compared to those reported previous TX/RX systems. The digital-to-impulse radiating array in CMOS, [11] is not included in this comparison, because such a TX was not evaluated for high-resolution gas spectroscopy (requiring spectroscopy at a low gas pressure of few Pa) according to the available literature.

The simulated antenna efficiency is at 240 GHz of -4.3 dB, and at 480 GHz of -5.3 dB, and thus lower compared to the -1.9 dB (65%) efficiency at 240 GHz for our previous TX with a bowtie antenna on silicon lens [26]. But, the efficiency of the dual-polarization antenna could be increased by 2-3 dB by applying differential transmission lines of a wider width, as e.g., of 7 μm.

We have demonstrated the performance of the system for gas spectroscopy by taking reference spectra of methanol at 5 Pa in the two frequency ranges. We have observed an SNR of 1700 at 241.7 GHz (line intensity $5{\cdot}10^{-23}$ $cm^{-1}/(molecule{\cdot}cm^{-2})$) for 16 ms integration time. This corresponds to a minimum detectable absorption coefficient of 4.10^{-7} cm^{-1} for an absorption length of 1.9 m. Typical detection limits resulting from that are in the ppb to ppm range as derived previously for a similar system [41]. With 2 ms integration time, the SNR of this line is 730. This is smaller compared to our previous publication with an SNR of 6000 for an integration time of 2 ms, see [26], due to the lower TX output power and the smaller antenna gain. The SNR in the upper frequency band is considerably lower, as expected due to the lower TX output power and the higher NF of the RX, see Table 3. At 483.539 GHz (line intensity $2{\cdot}10^{-22}$ $cm^{-1}/(molecule{\cdot}cm^{-2})$) we have determined an SNR of 50 (2 ms integration time). Considering the line intensities, the sensitivity of the system is roughly 60 times (18 dB) higher in the lower frequency band. This corresponds roughly with our expectations due to the lower power of the TX (∼−10 dB), which scales with the SNR by the square root, and the higher

noise figure (~ -15 dB) compared to the lower frequency band.

Note, that the SNR could be increased for the higher frequency band by a narrower bandwidth of the IF bandpass filter than the used 200 MHz, e. g. by 10 dB for a 20 MHz bandwidth. Further, the TX output-power could be increased by a 4-way combined frequency multiplier, [27] in its 480 GHz branch instead the used one-way frequency multiplier, e. g. by about 5 dB at 480 GHz. However, the TX DC-power would be higher by 1.4 W. Note also, that for a detailed comparison, many more parameters such as the alignment or standing waves, have to be analyzed and taken into account. However, the extension of the frequency range is valuable for gas spectroscopy, since many molecules can be detected exclusively or more sensitively in the upper frequency band due to stronger absorption lines.

V. CONCLUSION

We presented a two-band TX/RX system in SiGe BiCMOS technology for gas spectroscopy at 222–270 GHz and the doubled frequency at 444–540 GHz, and discussed its performance in relation to the implemented cross-polarized bowtie-antenna on silicon-lens.

Our spectroscopy system will be further developed in order to increase the TX power above 500 GHz for higher sensitivity.

ACKNOWLEDGMENT

The authors would like to thank Volker Mühlhaus, Dr. Mühlhaus Consulting & Software GmbH, for his valuable support for software EMPIRE XPU. They are also grateful to Thomas Mausolf, IHP, for on-wafer measurements of test-structures.

REFERENCES

[1] I. R. Medvedev, C. F. Neese, G. M. Plummer, and F. C. De Lucia, "Submillimeter spectroscopy for chemical analysis with absolute specificity," *Opt. Lett.*, vol. 35, no. 10, pp. 1533–1535, 2010.

[2] C. F. Neese, I. R. Medvedev, G. M. Plummer, A. J. Frank, C. D. Ball, and F. C. De Lucia, "Compact submillimeter/terahertz gas sensor with efficient gas collection, preconcentration, and ppt sensitivity," *IEEE Sensors J.*, vol. 12, no. 8, pp. 2565–2574, Aug. 2012.

[3] A. M. Fosnight, B. L. Moran, and I. R. Medvedev, "Chemical analysis of exhaled human breath using a terahertz spectroscopic approach," *Appl. Phys. Lett.*, vol. 103, no. 13, 2013, Art. no. 133703.

[4] C. Wang and R. Han, "Dual-terahertz-comb spectrometer on CMOS for rapid, wide-range gas detection with absolute specificity," *IEEE J. Solid-State Circuits*, vol. 52, no. 12, pp. 3361–3372, Dec. 2017.

[5] C. Wang, B. Perkins, Z. Wang, and R. Han, "Molecular detection for unconcentrated gas with ppm sensitivity using dual-THz-comb spectrometer in CMOS," *IEEE Trans. Biomed. Circuits Syst.*, vol. 12, no. 3, pp. 709–721, Jun. 2018.

[6] N. Sharma et al., "200–280 GHz CMOS RF front-end of transmitter for rotational spectroscopy," in *Proc. IEEE Symp. VLSI Technol.*, 2016, pp. 1–2, doi: 10.1109/VLSIT.2016.7573400.

[7] Q. Zhong, W. Choi, C. Miller, R. Henderson, and K. O. Kenneth, "A 210-to-305 GHz CMOS receiver for rotational spectroscopy," in *Proc. IEEE Int. Solid-State Circuits Conf.*, 2016, pp. 426–427, doi: 10.1109/ISSCC.2016.7418089.

[8] N. Sharma et al., "Complementary metal oxide semiconductor integrated circuits for rotational spectroscopy," in *Proc. SPIE, Next-Gener. Spectroscopic Technol. XIII*, 2020, pp. 1–17.

[9] D. J. Nemchick et al., "180 GHz pulsed CMOS transmitter for molecular sensing," *IEEE Trans. THz Sci. Technol.*, vol. 11, no. 5, pp. 469–476, Sep. 2021, doi: 10.1109/TTHZ.2021.3085138.

[10] Y. Kim et al., "A 183-GHz inp/CMOS-hybrid heterodyne-spectrometer for spaceborne atmospheric remote sensing," *IEEE Trans. THz Sci. Technol.*, vol. 9, no. 3, pp. 313–334, May 2019.

[11] M. M. Assefzadeh et al., "Terahertz trace gas spectroscopy based on a fully-electronic frequency-comb radiating array in silicon," in *Proc. Conf. Lasers Electro-Opt.*, 2016, pp. 1–2.

[12] S. Razavian, M. Hosseini, Y. Mehta, and A. Babakhani, "Terahertz channel characterization using a broadband frequency comb radiator in 130-nm SiGe BiCMOS," *IEEE Trans. THz Sci. Technol.*, vol. 11, no. 3, pp. 269–276, May 2021, doi: 10.1109/TTHZ.2021.3059335.

[13] K. Schmalz et al., "500 GHz sensor system in SiGe for gas spectroscopy," in *Proc. 40th Int. Conf. Infrared, Millimeter, THz Waves*, 2015, pp. 1–2, doi: 10.1109/IRMMW-THz.2015.7327489.

[14] K. Schmalz et al., "Tunable 500 GHz sensor system in SiGe technology for gas spectroscopy," *Electron. Lett.*, , vol. 51, no. 17, pp. 1345–1347, Aug. 2015.

[15] K. Schmalz, Y. Mao, J. Borngräber, P. Neumaier, and H.-W. Hübers, "Tunable 245 GHz transmitter and receiver in SiGe technology for gas spectroscopy," *Electron. Lett.*, vol. 50, no. 12, pp. 881–882, Jun. 2014.

[16] K. Schmalz, P. Neumaier, J. Borngräber, W. Debski, and H.-W. Hübers, "245 GHz transmitter and receiver in SiGe for gas spectroscopy," in *Proc. 39th Int. Conf. Infrared, Millimeter, THz Waves*, 2014, pp. 1–2.

[17] K. Schmalz et al., "245-GHz transmitter array in SiGe BiCMOS for gas spectroscopy," *IEEE Trans. THz Sci. Technol.*, vol. 6, no. 2, pp. 318–327, Mar. 2016.

[18] K. Schmalz, N. Rothbart, P. F.-X. Neumaier, J. Borngräber, H.-W. Hübers, and D. Kissinger, "Gas spectroscopy system for breath analysis at mmwave/THz using SiGe BiCMOS circuits," *IEEE Trans. Microw. Theory Techn.*, vol. 65, no. 5, pp. 1807–1818, Jan. 2017.

[19] K. Schmalz et al., "245 GHz SiGe sensor system for gas spectroscopy," *Int. J. Microw. Wireless Technol.*, vol. 7, no. 3/4, pp. 271–278, 2015.

[20] K. Schmalz et al., "245 GHz SiGe transmitter with integrated antenna and external PLL," in *IEEE MTT-S Int. Microw. Symp. Dig.*, 2013, pp. 1–4.

[21] K. Schmalz, J. Borngräber, P. Neumaier, H. Hübers, and D. Kissinger, "A 245 GHz transmitter in SiGe technology," in *Proc. IEEE Radio Freq. Integr. Circuits Symp.*, 2012, pp. 195–198.

[22] K. Schmalz, J. Borngräber, P. Neumaier, H. Hübers, and D. Kissinger, "Sensor system in sige BiCMOS at 245 and 500 GHz for gas spectroscopy," in *Proc. IEEE 16th Topical Meeting Silicon Monolithic Integr. Circuits RF Syst.*, 2016, pp. 70–72.

[23] K. Schmalz, J. Borngräber, P. Neumaier, N. Rothbart, D. Kissinger, and H. Hübers, "Gas spectroscopy system at 245 and 500 GHz using transmitters and receivers in SiGe BiCMOS," in *Proc. Glob. Symp. Millimeter Waves ESA Workshop Millimetre-Wave Technol. Appl.*, 2016, pp. 1–4.

[24] K. Schmalz et al., "Gas spectroscopy system with transmitters and receivers in SiGe BiCMOS for 225–273 GHz," *Proc. SPIE*, vol. 10439, 2017, Art. no. 1043902.

[25] K. Schmalz, N. Rothbart, M. H. Eissa, J. Borngräber, D. Kissinger, and H.-W. Hübers, "Transmitters and receivers in SiGe BiCMOS technology for sensitive gas spectroscopy at 222–270 GHz," *AIP Adv.*, vol. 9, 2019, Art. no. 015213.

[26] K. Schmalz et al., "Dual-band transmitter and receiver with bowtie-antenna in 0.13 μm SiGe BiCMOS for gas spectroscopy at 222–270 GHz," *IEEE Access*, vol. 9, pp. 124805–124816, 2021, doi: 10.1109/ACCESS.2021.3110210.

[27] A. Güner, T. Mausolf, J. Wessel, D. Kissinger, and K. Schmalz, "A 440–540-GHz transmitter in 130-nm SiGe BiCMOS," *IEEE Microw. Wireless Compon. Lett.*, vol. 31, no. 6, pp. 779–782, Jun. 2021, doi: 10.1109/LMWC.2021.3060820.

[28] A. Güner, T. Mausolf, J. Wessel, D. Kissinger, and K. Schmalz, "A 440–540-GHz subharmonic mixer in 130-nm SiGe BiCMOS," *IEEE Microw. Wireless Compon. Lett.*, vol. 30, no. 12, pp. 1161–1164, Dec. 2020, doi: 10.1109/LMWC.2020.3030315.

[29] [Online]. Available: https://www.ihp-microelectronics.com/

[30] K. Schmalz, J. Borngräber, B. Heinemann, H. Rücker, and J. C. Scheytt, "A 245 GHz transmitter in SiGe technology," in *Proc. IEEE Radio Freq. Integr. Circuits Symp.*, 2012, pp. 195–198, doi: 10.1109/RFIC.2012.6242262.
[31] M. H. Eissa et al., "A 220–275 GHz direct-conversion receiver in 130-nm SiGe:C BiCMOS technology," *IEEE Microw. Wireless Compon. Lett.*, vol. 27, no. 7, pp. 675–677, Jul. 2017.
[32] M. H. Eissa et al., "Wideband 240-GHz transmitter and receiver in BiCMOS technology with 25-Gbit/s data rate," *IEEE J. Solid-State Circuits*, vol. 53, no. 9, pp. 2532–2542, Sep. 2018.
[33] J. Grzyb, K. Statnikov, N. Sarmah, B. Heinemann, and U. R. Pfeiffer, "A 210–270-GHz circularly polarized FMCW radar with a single-lens-coupled SiGe HBT chip," *IEEE Trans. THz Sci. Technol.*, vol. 6, no. 6, pp. 771–783, Nov. 2016.
[34] J. Grzyb, K. Statnikov, N. Sarmah, and U. R. Pfeiffer, "A broadband 240 GHz lens-integrated polarization-diversity on-chip circular slot antenna for a power source module in SiGe technology," in *Proc. Eur. Microw. Conf.*, 2015, pp. 570–573, doi: 10.1109/EuMC.2015.7345827.
[35] P. Rodriguez-Vazquez, J. Grzyb, B. Heinemann, and U. R. Pfeiffer, "A QPSK 110-Gb/s polarization-diversity MIMO wireless link with a 220–255 GHz tunable LO in a SiGe HBT technology," *IEEE Trans. Microw. Theory Techn.*, vol. 68, no. 9, pp. 3834–3851, Sep. 2020, doi: 10.1109/TMTT.2020.2986196.
[36] [Online]. Available: https://www.ansys.com/
[37] [Online]. Available: https://empire.de/
[38] [Online]. Available: https://www.cadence.com/
[39] J. E. Hill, *Gain of Directional Antennas*, Palo Alto, CA, USA: Watkins-Johnson, 1976.
[40] N. Rothbart, O. Holz, R. Koczulla, K. Schmalz, and H.-W. Hübers, "Analysis of human breath by millimeter-wave/terahertz spectroscopy," *Sensors*, vol. 19, 2019, Art. no. 2719, doi: 10.3390/s19122719.
[41] N. Rothbart, K. Schmalz, and H.-W. Hübers, "A compact circular multipass cell for millimeter-wave/terahertz gas spectroscopy," *IEEE Trans. THz Sci. Technol.*, vol. 10, no. 1, pp. 9–14, Jan. 2020.

KLAUS SCHMALZ received the Ph.D. degree in physics in 1978. He worked in the field of silicon semiconductor technologies and research for some time and has expertise in the area of thermally induced defects and characterization of Si/SiGe structures. After training in RF circuit design at UCLA in Los Angeles (1998–1999), he changed his scientific focus to RF analog circuit design. His research interests include the design of SiGe BiCMOS analog circuits for wireless communication with emphasis on RF front-ends for different standards and mm-wave circuits for sensor applications. He has authored or coauthored more than 100 papers. He is currently with IHP, Frankfurt (Oder).

ALEXANDRA GLÜCK was born in Karlsruhe, Germany, in 1995. She received the B.Sc. degree in physics from the University of Freiburg, Freiburg, Germany, in 2016, and the M.Sc. degree in physics from Humboldt-Universität zu Berlin, Berlin, Germany, in 2019. She is currently working toward the Dr.rer.nat. degree in physics with German Aerospace Center in Berlin, Germany. Her work focuses on high resolution gas spectroscopy at GHz frequencies.

NICK ROTHBART received the Master of Science degree in physics from the Humboldt-Universität zu Berlin, Berlin, Germany, in 2011, and the Dr. rer.nat degree in physics from the Technische Universität Berlin, Berlin, Germany, in 2015, for his work on security-relevant terahertz imaging and spectroscopy that was accomplished at the German Aerospace Center (DLR) in Berlin and supported by a scholarship and membership with the Helmholtz Research School on Security Technologies (HRSST). From 2014 to 2015, he was also with the Federal Institute for Materials Research and Testing (BAM). Since 2015, he has been involving in mmW/THz gas spectroscopy with DLR and Humboldt-Universität zu Berlin.

ALPER GÜNER received the B.S. and M.S. degrees in electronical engineering from Sabanci University, Istanbul, Turkey, in 2016 and 2018, respectively. His M.S. studies focused on full duplex Ka-band transceivers for 5G applications. In 2018, he joined IHP Microelectronics as a Scientist and an integrated Circuit Designer. His research interests include developing sub-terahertz circuits and systems for gas spectroscopy and short range radar applications.

MOHAMED HUSSEIN EISSA received the B.Sc. degree in electrical engineering from Ain Shams University, Cairo, Egypt, in 2009, the M.Sc. degree in electronics and communications from The American University in Cairo, Cairo, Egypt, in 2014, and the Ph.D. degree from the Technical University of Berlin, Berlin, Germany, in 2019. For two years, he was with Silicon Vision LLC., Cairo, Egypt, involved in the design of ASICs for low power Bluetooth communication standard. From 2011 to 2014, he joined Hittite Microwave, Cairo, Egypt, working on the design of transceivers for point to point communication. Since October 2014, he has been with IHP, Germany, as a Research Scientist with the Circuit Design Department. His research interests include RF and mm-wave circuit designs for communication and radar applications.

HEINZ-WILHELM HÜBERS received the Diploma and the Dr.rer.nat. degree in physics from Universität Bonn, Bonn, Germany, in 1991 and 1994, respectively. From 1991 to 1994, he was with Max-Planck-Institut für Radioastronomie, Bonn, Germany. In 1994, he joined Deutsches Zentrum für Luft-und Raumfahrt (German Aerospace Center, DLR), Berlin, Germany, becoming the Head of the Department in 2001. From 2009 to 2014, he was a Professor of experimental physics with Technische Universität Berlin, Germany, and the Head of the Department Experimental Planetary Physics, DLR. In 2014, he became the Director of the DLR's Institute of Optical Sensor Systems and a Professor with Humboldt-Universität zu Berlin, Berlin, German. His research interests include THz physics and spectroscopy, particularly in THz systems for astronomy, planetary research, and security. Prof. Hübers was the recipient of the Innovation Award on Synchrotron Radiation (2003) and the Lilienthal Award (2007). In 2021, he received an honorary doctorate at Chalmers University of Technology, Gothenburg, Sweden.